Modeling the Thermal-Mechanical Behavior of Mid-Ocean Ridge Transform Faults

Emily C Roland[*1], Mark Behn[,2] and Greg Hirth[3]
[1]MIT/WHOI Joint Program, [2]Woods Hole Oceanographic Institution, [3]Brown University
*Woods Hole Oceanographic Inst. MS 24; Woods Hole, MA 02543, eroland@mit.edu

Abstract: To investigate the thermal-mechanical behavior of oceanic transform faults, we calculate 3-D steady-state incompressible mantle flow and heat transport using COMSOL Multiphysics 3.2. Our model incorporates a non-linear viscous rheology with a visco-plastic approximation to simulate lithospheric brittle failure. We incorporate the effects of hydrothermal circulation and changes in frictional behavior due to mantle alteration. By examining a rage of parameters, including the slip rate along the fault and the efficiency of hydrothermal circulation, we characterize the thermal structure and stress state surrounding transform faults. These results provide new constraints on the size of seismogenic zone at oceanic transform faults and the degree of hydration of the oceanic upper mantle.

Keywords: fault mechanics, tectonics, fluid dynamics, plasticity, dislocation creep

1. Introduction

Oceanic transform faults represent localized zones of shear deformation in the Earth's crust and upper mantle similar to strike-slip faults in continental regions (e.g., San Andreas and Northern Anatolian faults). Transforms are ubiquitous features of the sea-floor ridge system, forming to accommodate the relative strike-slip motion between adjacent mid-ocean ridge spreading segments.

Various geodynamical processes are influenced by oceanic transform faults. Earthquake behavior and other faulting processes are directly linked to the thermal structure and mechanical nature of the transform. Strain along the fault influences flow in the upper oceanic mantle, and leads to regions of increased permeability, providing a mechanism for water to be transported into the crust and mantle. Fluid circulation in the oceanic lithosphere promotes hydrothermal cooling, as well as the formation of hydrous metamorphic minerals where water comes into contact with mantle rocks. Improved characterization of these processes will have a direct bearing on models of the ridge-transform tectonic systems and ridge-subduction zone interactions.

To investigate the thermal-mechanical behavior of oceanic transform faults and the influence they have on mantle flow and lithospheric processes in the shallow earth, we utilize COMSOL Multiphysics 3.2 to simulate 3-D steady-state incompressible mantle flow and advective and conductive heat transport. Our models incorporate a non-linear viscous rheology with a visco-plastic approximation to simulate brittle failure. We also incorporate the effects of hydrothermal circulation and changes in frictional behavior due to mantle alteration. Through examining a range of parameters, including the slip rate on the fault and the efficiency of hydrothermal circulation, we constrain the first-order thermal structure and zone of permeable fluid flow.

2. Physical Background

Previous studies of transform fault thermal structure incorporate conductive and advective heat transport using a constant or temperature-dependent viscosity. Thermal solutions derived from these models produce faults that are cooler than the surrounding plate (Morgan & Forsyth 1988; Shen & Forsyth 1992). While these models take into account realistic heat flow processes, the resulting cool fault structure is generally inconsistent with seismologic observations and frictional behavior of fault rocks derived from laboratory experiments (Abercrombie & Ekstrom 2001; Boettcher, Hirth & Evans 2007). These inconsistencies are likely related to the lack of brittle failure mechanisms incorporated in the models. In the shallow lithosphere where faulting occurs, temperatures are too cold to permit viscous deformation on short time-scales, and brittle processes dominate the deformation and stress regime. Here, we

have incorporated a plastic approximation in our viscous rheology that accounts for deformation from applied stress that is retained as opposed to viscously relaxed. This plasticity thus provides for upper lithospheric brittle processes that are important for realistic models of fault thermal structure.

3. Numerical Model

3.1 Model Setup

We use COMSOL 3.2 to solve for the 3-D steady-state viscous mantle flow and temperature structure surrounding oceanic transform faults. Within our model, mantle flow is driven by imposing horizontal surface velocities parallel to a fault, simulating plate velocity for a number of slip rates between 3 and 12 cm/yr. The top and bottom surfaces of the model space are set to a surface temperature (T_s) of 0˚C and a mantle temperature (T_m) of 1300˚C, respectively. The sides and bottom of the model are stress free, allowing convective flux in and out of the model space, and providing for mantle upwelling from below. Here, we examine a 100 km long transform fault, offsetting a ridge that extends 50 km on either side of the fault (*Fig. 1*). A rectangular mesh has been used for all solutions presented here with finer resolution in the regions surrounding the transform fault and at the ridge ends.

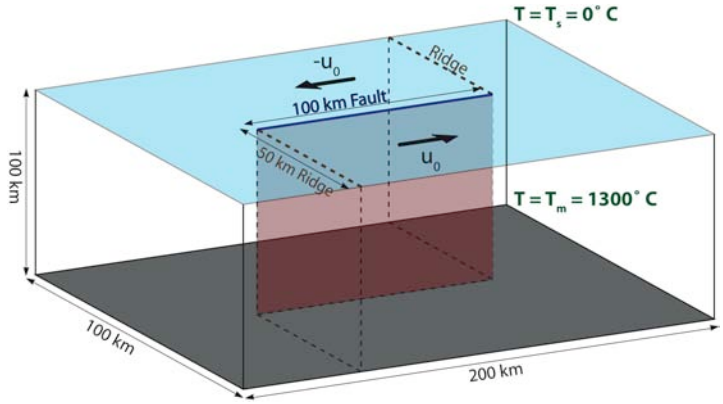

Figure 1. Schematic illustration of the model geometry as developed using COMSOL 3.2 finite element software.

3.2 Governing Equations

We solve for conservation of mass and momentum following:

$$u \cdot \nabla = 0 \qquad (1)$$

$$\rho(u \cdot \nabla)u = \nabla \cdot \left[-pI + \eta\left(\nabla u + (\nabla u)^T\right)\right], \qquad (2)$$

where u is velocity, ρ is density and p is pressure. Equation (2) equates the change in momentum to the sum of the pressure gradient and the dissipative forces. We also solve the heat transport equation:

$$\nabla \cdot (-k\nabla T) = Q - \rho C_p u \cdot \nabla T, \qquad (3)$$

which allows for heat diffusion as well as convective heat flow. In Equation (3), T is temperature, Q is the heat flow, C_p is specific heat and k is the thermal conductivity. Basic model perameters and values of specific properties used in our simulations are given in *Tables 1 and 2*.

Table 1: Basic Model Parameters

x	*transform-parallel axis*
y	*transform-normal axis*
z	*depth axis*
u	*flow velocity*
T	*temperature*
η	*effective viscosity*
$\dot{\varepsilon}$	*strain-rate*
P	*pressure*
σ_n	*normal stress*
τ	*maximum shear stress*

4. Constitutive Equations

4.1 Visco-plastic Rheology

Following Chen and Morgan, (1990) we calculate the temperature and stress fields using a non-linear viscous-plastic rheology that allows for brittle weakening in the lithosphere. Where temperatures are sufficiently high for rocks to deform by dislocation creep, we adopt a power-law dependence of strain-rate on differential stress (Kirby 1983):

$$\dot{\varepsilon} = A(\sigma_1 - \sigma_3)^n \exp\left(-\frac{E}{RT}\right). \quad (4)$$

where, $\dot{\varepsilon}$ is strain-rate, σ_1 and σ_3 are the maximum and minimum principal stresses respectively, R is the gas constant, and A, n and E are material properties (*Table 2*). Values for these parameters are consistent with a dry olivine composition (Hirth & Kohlstedt 2003). We incorporate this relation into our model in the form of a stress and strain-rate dependent viscosity, η_{disl}, derived using the relation between the isotropic stress tensor and the strain-rate tensor:

$$\sigma_{ij} = 2\eta\dot{\varepsilon}. \quad (5)$$

This allows us to calculate viscosity as a function of the second invariant of the strain-rate, $\dot{\varepsilon}_{II}$, as:

$$\eta_{disl} = B\,\dot{\varepsilon}_{II}^{\left(\frac{1-n}{n}\right)} \exp\left(\frac{E}{nRT}\right), \quad (6)$$

where

$$B = \frac{1}{4}\left(\frac{4}{3A}\right)^{1/n}. \quad (7)$$

In the lithosphere, where cold temperatures would produce unrealistically high viscosities, deformation is accommodated by brittle mechanisms (e.g., faulting). Amonton's law has been developed from the observation that, for most rocks under a wide range of stress states, yielding will occur as a linear function of normal stress:

$$\tau = \mu\bar{\sigma}_n + C, \quad (8)$$

here expressed in terms of the shear stress, τ, at which frictional sliding begins; the effective normal stress, $\bar{\sigma}_n$; the coefficient of friction, μ; and the cohesive strength of the rock, C -(*Table 2*). At low normal stress, rocks typically have a value of $\mu = 0.85$ (e.g., Byerlee, 1978). Pore fluid pressure, P_p, acts to oppose the normal stress, resulting in the following equation for the effective normal stress:

$$\bar{\sigma}_n = \sigma_n - P_p. \quad (9)$$

Because our models are referenced from the seafloor and we assume the lithosphere near the mid-ocean ridge is under ridge-normal extension, the maximum principal effective compressive stress, $\bar{\sigma}_1$, is simply the effective overburden, or the lithostatic stress reduced by the pore-fluid pressure. In terms of principal compressive stresses, combining equations (8) and (9) results in:

$$\tau = \frac{2}{5}\bar{\sigma}_1, \quad \bar{\sigma}_1 = (\rho - \rho_h)gz, \quad (10)$$

when $\mu = 0.85$ and $C = 0$, with ρ, ρ_h, g and z, the rock density, the water density, gravity and the depth below the seafloor, respectively (*Table 2*). Equation (10) represents the maximum shear stress the plate can support before brittle failure, and is used to limit the maximum shear stress in the shallow, cool lithosphere.

Table 2: Boundary conditions and material properties

u_0	*imposed half slip rate*	1.5-6 cm yr^{-1}
T_s	*surface temperature*	0 ˚C
T_m	*mantle temperature*	1300 ˚C
C	*cohesion*	20 MPa
μ	*coefficient of friction*	0.85, 0.1
C_p	*specific heat*	1000 J Kg^{-1} ˚K^{-1}
k	*thermal conductivity*	3 W m^{-1} ˚K^{-1}
E	*activation energy*	520 kg mol^{-1} (Hirth & Kohlstedt)
n	*stress exponent*	3.5 (Hirth & Kohlstedt)
A	*pre-exponential factor*	1.1x10^5 (Hirth & Kohlstedt)
R	*gass constant*	8.3145 J mol^{-1} ˚K^{-1}
ρ	*average lithospheric density*	3300 kg m^{-3}
ρ_h	*water density*	1000 kg m^{-3}
Nu	*Nusselt number*	1-10
g	*gravity*	9.8 m s^{-1}

A composite rheology law is used to incorporate both viscous and plastic deformation mechanisms into our model. This composite rheology is constrained in our solution process through an effective viscosity. Based on our calculated yield stress, we derive a "brittle viscosity":

$$\eta_{brittle} = \frac{\tau}{\sqrt{2}\,\dot{\varepsilon}}. \qquad (11)$$

The brittle viscosity is combined in parallel with our power-law viscosity, η_{disl}, calculated from Equation (6), and a maximum cutoff viscosity, $\eta_{\max}$, to obtain the effective viscosity used in the flow calculations:

$$\eta_{eff} = \left(\frac{1}{\eta_{brittle}} + \frac{1}{\eta_{disl}} + \frac{1}{\eta_{\max}} \right)^{-1}. \qquad (12)$$

We include the maximum cutoff viscosity, $\eta_{\max}$ to facilitate numerical convergence where small values of strain-rate result in very large viscosity gradients. This maximum value is iteratively increased until it no longer affects the solution. Within the expression for effective viscosity, the smallest viscosity term dominates, reflecting the most favorable deformation mechanism. Adopting this method for combining our brittle failure law with our viscous law smoothes the 'beak' of the stress profile near the brittle-ductile transition (*Fig. 2a*) and aids with numerical stability.

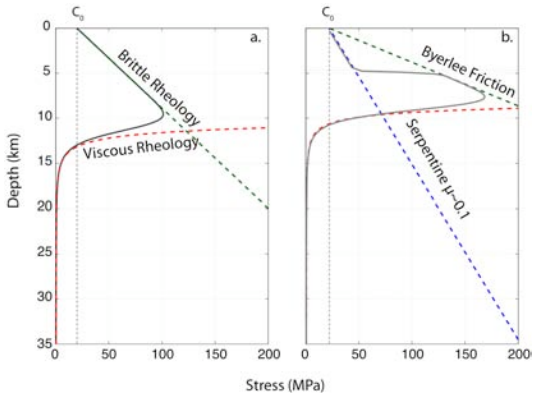

Figure 2. Shear stress-depth profiles illustrating visco-plastic composite rheology (black lines). **(a)** Brittle mechanisms described by Amaton's law (green) dominant at shallow depths, and the non-linear viscous dislocation creep law (red) dictates deformation at depth. **(b)** Incorporation of a weakened serpentine rheology with $\mu = 0.1$. In zones where metamorphic alteration is likely to occur, the serpentine rheology will dominate the brittle failure (blue). Black curves show composite effective viscosity profiles.

4.2 Rheological Feedbacks - *weakening due to alteration*

In the shallow mantle where we expect deformation in the oceanic lithosphere to occur by brittle mechanisms, metamorphic alteration from circulating fluids may affect the frictional strength. In the presence of water, mantle peridotite will alter to the hydrous mineral phases serpentine and talc depending on the pressure and temperature conditions. Laboratory studies show that rocks with even a small degree of serpentinization are significantly weaker than unaltered olivine (Escartin, G. Hirth & Evans 2001). These alteration products can exhibit coefficients of friction as low as 0.1 (Moore et al. 1997). We include a rheological feedback, taking into account the change in strength that occurs due to metamorphic alteration where brittle failure leads to increased permeability and fluid infiltration.

Zones of alteration are estimated based on phase stability fields for water-saturated peridotites (Poli and Schmit, 2002). We assume rock strength is reduced in regions of brittle failure within the pressure and temperature limits of the serpentine and talc stability fields. In these regions, the brittle rheology law in Equation (10) is adjusted to reflect the reduced coefficient of friction, from the typical dry olivine value of 0.85 to 0.1 (O'Hanley 1996; Escartin, G. Hirth & Evans 2001). An illustration of the shear stress-depth profile for the composite visco-plastic rheology with weak zones of serpentinization is illustrated in *Figure 2b*.

4.3 Thermal Feedbacks*: hydrothermal cooling*

In the upper lithosphere, fluid convection through regions of increased permeability acts as an additional mechanism for heat transfer. We approximate the effect of hydrothermal circulation by increasing thermal conductivity in regions where we would expect fluids to circulate (e.g. Phipps Morgan, Parmentier & Lin 1987). This increase takes the form of a Nusselt number, *Nu*, which is the ratio of the total heat transport within a permeable layer to heat

transfer by conduction alone (Morgan & Chen 1993). We investigated a range of Nusselt numbers, $Nu = 1-10$, which imply different efficiencies of hydrothermal cooling. Because fluids only circulate within interconnected conduits, the extent of hydrothermal circulation is limited by the region of brittle deformation and the overburden pressure. Permeability is only expected where brittle cracks form, and is predicted to decrease exponentially as overburden pressure increases with depth (David et al. 1994). Here, we define the zone of hydrothermal cooling as a function of both the depth of brittle deformation and the overburden pressure:

$$k_{eff} = \left(1 + (Nu - 1) \times erf(z - z_{brittle}) \times \exp\left(\frac{z}{z_{ref}}\right)\right) \times k$$

(*Equation 13*). The effective conductivity, k_{eff}, is increased by a factor, Nu, within the regions of most vigorous hydrothermal circulation, and decreases to its reference value, k as connected pores collapse due to overburden pressure. Permeability is assumed to be negligible below $z_{ref} = 6km$. At the maximum depth of brittle deformation, $z_{brittle}$, any increase in effective conductivity not reduced by overburden is smoothed via an error function to its value for intact rocks.

Profiles illustrating how our Nusselt number method simulates hydrothermal circulation for both warm/thin and cold/thick lithosphere are shown in *Figure 3*. Because brittle deformation extends to greater depths in thick, cold lithosphere, hydrothermal cooling is predicted to decrease exponentially with the overburden pressure down to 6 km. In warmer and thin lithosphere, where only a shallow zone deforms brittly, increases in thermal conductivity due to hydrothermal circulation are limited to the shallow brittle zone, decreasing smoothly across the maximum brittle depth to its reference value.

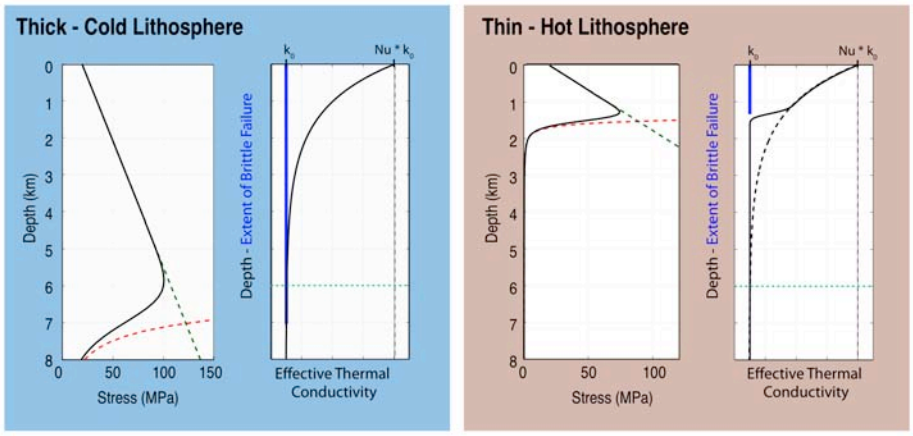

Figure 3. Schematic illustrating the increase in thermal conductivity used to simulate hydrothermal cooling **(a)** in zones of cool, thick lithosphere, and **(b)** in zones of the hot, thin lithosphere.

5. Modeling Results

For all model solutions, we find that incorporating a non-linear visco-plastic rheology leads to a transform fault domain that is warmer than the surrounding lithosphere (*Fig. 4*). These results differ from previous models with a constant or temperature dependent viscous rheology and no plasticity, which show transforms to be regions of anomalously cold lithosphere (e.g. Morgan & Forsyth 1988; Shen & Forsyth 1992). The warmer fault solution results from shear along the transform boundary - imposed as a kinematic boundary condition - leading to high strain rates along the fault. These high strain rates lead to brittle yielding and a lower effective viscosity in the shallow lithosphere. Models that consider viscous processes alone predict high stresses and viscosities at shallow depths, which act to inhibit mantle upwelling beneath the transform fault and result in a cooler thermal structure. In our

models, the reduced effective viscosity promotes passive mantle upwelling and increased heat transport upward from the hot mantle.

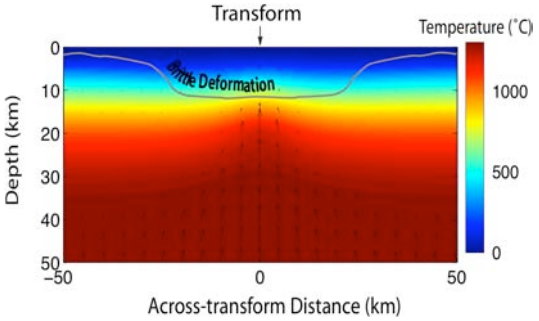

Figure 4. Temperature profile perpendicular to the center of a 100 km slow-slipping transform fault (slip rate = 3 cm/yr) and with a high degree of hydrothermal circulation (*Nu = 8)*. Gray line displays maximum depth of brittle deformation. Flow arrows (black) indicated enhanced mantle upwelling.

A profile of the temperature field across the center of a slow-slipping, 100-km transform fault derived from our visco-plastic rheology is shown in *Figure 4*. Isotherms shallow toward the center of the fault, illustrating the effect of the enhanced mantle upwelling. We investigate changes in the thermal structure for a series of model runs with different slip rates and efficiencies of hydrothermal circulation. The maximum depth of brittle failure and the average width of the brittle zone increase by as much as 20–30% as slip rate decreases from 12 to 3 cm/yr (*Figure 5*). These results are consistent with our understanding of how increased rates of passive mantle upwelling at faster spreading ridges generate warmer faults and ultimately smaller zones of brittle deformation, as is observed in the morphology of fast and slow spreading ridges.

Model results for variable *Nu* values suggest that hydrothermal circulation, and to a lesser degree, weakening due to metamorphic alteration, also affect transform thermal structure. Models show that more vigorous hydrothermal flow (i.e., higher Nusselt number), leads to cooler transform faults and progressively larger zones of brittle deformation (*Fig. 5*). Specifically, the extent of brittle failure is increased by 15–25% in depth, and by as much as 30% in width for Nu = 8 compared to models with no fluid circulation (Nu = 1).

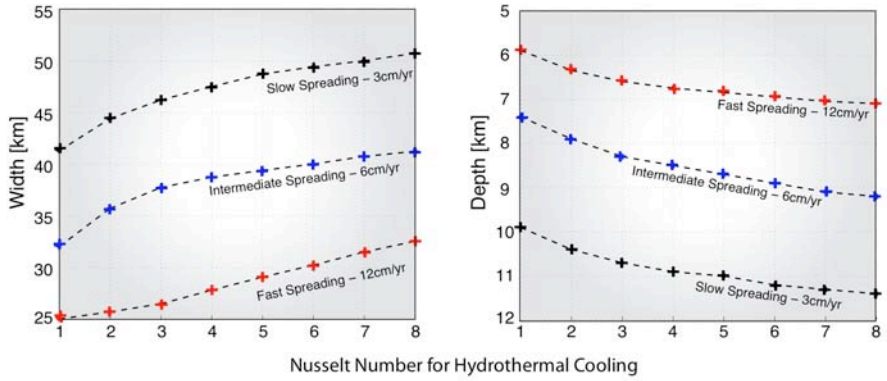

Figure 5. Summary of the change in the width and the depth of the brittly deforming zone for model solutions with different slip rates and values of Nusselt number. Red, blue, and black symbols represent results from individual model runs for slip rates of 12, 6, and 3 cm/yr, respectively.

In regions of the lithosphere where we expect hydrous minerals to form, the lower coefficient of friction of serpentine and talc phases leads to a reduction in the overall strength and effective viscosity, further promoting passive upwelling. Thermal solutions from these models reflect increases in passive upwelling, although the magnitude of the temperature increase is modest. For a 6 cm/year full-rate solution that incorporates the weakened serpentine rheology, temperatures increase a maximum of 12˚ C within a small shallow zone in the center of the transform. This rather small temperature change corresponds to a minor change in the predicted zone of brittle deformation, and a small increase in the maximum depth of brittle failure, on the

order of about 1% or 100 meters. Relative to the thermal feedback from hydrothermal cooling, the incorporation of the rheological feedback from metamorphic weakening has considerably smaller effect on the thermal solution.

6. Conclusions

We have developed numerical models of transform fault thermo-mechanical behavior with a rheology that allows for both viscous and brittle processes, and also incorporates specific thermal and rheological feedbacks known to be important in the ridge-transform fault setting. The effects of hydrothermal cooling and weakening due to metamorphic alteration have also been considered. We find that, the reduction in effective viscosity associated with plastic failure in regions of high strain rate, enhances passive mantle upwelling in these regions and leads to enhanced advection of heat to the transform domain. This generates a fault zone thermal structure that is warmer than the surrounding lithosphere. These results provide new constraints on the size of seismogenic zone at oceanic transform faults and the degree of hydration of the oceanic upper mantle.

8. References

1. Abercrombie, R.E. & Ekstrom, G., Earthquake slip on oceanic transform faults, *Nature*, **410**, 74-77, (2001)

2. Behn, M.D., Boettcher, M.S. & Hirth, G., Thermal structure of oceanic transform faults. *Geology*, **35**, 307-310 (2007)

3. Boettcher, M.S., Hirth, G. & Evans, B., Olivine friction at the base of oceanic seismogenic zones J. Geoph. Res., **112**, 1205. (2007)

4. David, C. et al., Laboratory measurement of compaction-induced permeability change in porous rocks: Implications for the generation and maintenance of pore pressure excess in the crust. *Pure and Applied Geophysics*, **143**, 425-456 (1994)

5. Escartin, J., Hirth, G. & Evans, B., Strength of slightly serpentinized peridotites: Implications for the tectonics of oceanic lithosphere. *Geology*, **29**, 1023-1026 (2001)

6. Hirth, G. & Kohlstedt, D.L., Rheology of the mantle wedge. *Inside the Subduction Factory, Geophysical Monograph*, **138**, 83–105(2003)

7. Kirby, S.H., Rheology of the Lithosphere (Paper 3R0741). *Rev. Geoph. Space Phy.*, **21**, 1458 (1983) 10.

8. Moore, D., D. Lockner, M. Shengli, R. Summers, and J. Byerlee, Strengths of serpentinite gouges at elevated temperatures *J. Geoph. Res*, **102** 14787-14801 (1997)

9. Morgan, J. & Chen, Y., The genesis of oceanic crust: Magma injection, hydrothermal circulation, and crustal flow. *J. Geoph. Res*, **98**, 6283–6298 (1993)

10. Morgan, J.P. & Forsyth, D.W., Three dimensional flow and temperature perturbations due to a transform offset: Effects on oceanic crustal and upper mantle structure. *J. Geoph. Res.,* **93**, 2955-2966 (1988)

11. O'Hanley D.S., Serpentinites: Recorders of Tectonic and Petrological History, Oxford University Press. (1996)

12. Phipps Morgan, J., Parmentier, E.M. & Lin, J., Mechanisms for the origin of Mid-Ocean Ridge axial topography: Implications for the thermal and mechanical structure of accreting plate boundaries. *J. Geoph Res.*, **92**, 12823-12836 (1987)

13. Poli, S. & Schmidt, M.W., Petrology of bducted Slabs. *Annu. Rev. Earth Planet. Sci*, **30**, 207-235 (2002)

14. Shen, Y. & Forsyth, D.W., The effects of temperature-and pressure-dependent viscosity on three-dimensional passive flow of the mantle beneath a ridge-transform system. *J. Geoph. Res.*, **97**, 19,717-19,728 (1992)